Laterally Confined Volcanic Successions (LCVS); recording rift-jumps during the formation of magma-rich margins

James R. Norcliffe[a]*, Douglas A. Paton[a], Estelle J. Mortimer[a], Andrew M. McCaig[a], Howard Nicholls[b], Karyna Rodriguez[b], Neil Hodgson[b], David Van Der Spuy[c]

[a]School of Earth and Environment, University of Leeds, Leeds, LS2 9JT, United Kingdom

[b]Spectrum, Dukes Court, Woking ,GU21 5BH, United Kingdom

[c]Petroleum Agency South Africa, Bellville 7530, Cape Town, South Africa

* Corresponding author: ee13jrn@leeds.ac.uk

Abstract

Seaward Dipping Reflectors (SDRs) are a characteristic feature of magma-rich margins, and represent the generation of large volumes of flood basalts at the point of continental break-up. A number of recent studies provide new insights into the emplacement and tilting of SDRs and conclude that the majority of SDRs are contained within new magmatic crust that has a close affinity to oceanic crust. However, the process by which these initial magmatic systems evolve into a fully established spreading centre remains poorly understood. Several characteristic features of magma-rich margins may be explained by the occurrence of rift-jumps during SDR emplacement, yet the cause and prevalence of such rift-jumps remain unknown.

Here we constrain the 3D geometry of the continent-ocean transition in the Orange Basin, offshore South Africa. This allows us to test if, where and why such rift jumps occur. Our results demonstrate an order of along-strike segmentation previously unobserved in these settings. We demonstrate that the SDR belt is disrupted by the occurrence of a volcanic-stratigraphic package, defined as the Laterally Confined Volcanic Succession (LCVS), not previously identified on a rifted margin. We interpret this as a magmatic spreading centre that was abandoned by a subsequent rift-jump. Identification of LCVSs is important for two reasons. First, we argue that the LCVS formed via the same process as SDRs, and hence provides a unique example of SDR geometry prior to their separation onto conjugate plates. Second, as we can map out the 3D geometry of the LCVS and SDRs, we propose that rift-jumps during magma-rich margin formation may be fundamental to the establishment of a laterally continuous incipient spreading centre.

Keywords:

Volcanic margin, seaward dipping reflectors, rifting, South Atlantic

1. Introduction

Magma-rich margins form when continental breakup is accompanied by the emplacement of large volumes of igneous rock (White and McKenzie, 1989). The addition of magmatic material to the thinned continental crust has made these margins more difficult to study than their magma-poor counterparts, which are defined by detachment faulting, hyperextension and mantle exhumation (Manatschal, 2004; Péron-Pinvidic and Manatschal, 2008). Hence despite the widespread occurrence of magma-rich margins globally, many elements of their magmatic and tectonic evolution remain poorly understood.

In seismic reflection profiles, the diagnostic feature of magma-rich margins is the occurrence of thick sequences of seaward dipping reflectors (SDRs) in the upper crust (Hinz, 1981; Mutter et al., 1982; White and McKenzie, 1989). Drilling and geophysical studies (Eldholm and Grue, 1994; Jackson et al., 2000; Larsen and Saunders, 1998; Mutter et al., 1982; Planke and Eldholm, 1994) have consistently shown that SDRs consist predominantly of flood basalts. It has been demonstrated that the innermost SDRs were emplaced on top of attenuated and intruded continental crust (Larsen and Saunders, 1998) whilst the outermost SDRs were emplaced as the uppermost layer of thickened oceanic crust (Larsen and Saunders, 1998; Mutter et al., 1982; Paton et al., 2017). Therefore, the emplacement and tilting of SDRs record how tectonic and magmatic processes interact during the transition from continental thinning to seafloor spreading, and understanding their structural evolution is critical to understanding continental break-up. Several studies have used long-offset long-recording time 2D seismic reflection profiles to investigate SDR formation (e.g. Pindell et al., 2014; Quirk et al., 2014; McDermott et al., 2015; Paton et al., 2017), and these have been supported by numerical modelling (Buck, 2017; Corti et al., 2015) and field studies (Abdelmalak et al., 2015). These studies suggest that SDRs were originally emplaced as sub-horizontal lava flows in a magmatic zone located along the rift axis (e.g. Paton et al., 2017). Given the continued accretion of magmatic material in this zone, the older lava flows are transported away from the rift axis and develop axial dips. These dips form via a combination of magmatic loading and faulting (Buck, 2017; Clerc et al., 2015; Corti et al., 2015; Paton et al., 2017; Quirk et al., 2014).

Rift-jumps on fully established mid-ocean ridges occur across a range of scales, from 10’s (Hey, 1977) to 100’s (Mittelstaedt et al., 2011) km, and in response to local and regional processes. It has recently been suggested that repeated small rift-jumps (10’s km) also occur during SDR emplacement (Buck, 2017). Where rift-jumps, in this context, are defined as offsets in the location of the axial magmatic-zone. The occurrence of these events may play an important role in controlling the geometry and asymmetry of conjugate margins (Buck, 2017). However our understanding of the prevalence and driving mechanisms of such rift-jumps is currently limited, as is their impact on subsequent oceanic basin formation. Compounding this uncertainty is that current models only address SDR emplacement in two dimensions.

In this study we utilise a closely spaced 2D seismic reflection grid from the Orange Basin, offshore South Africa, to map the continent-ocean boundary in three dimensions. Specifically, we identify a new volcanic-stratigraphic package that resulted from a rift-jump during SDR emplacement. As this new packages records the abandonment of a magmatic spreading centre, it allow us to study the geometry of SDRs prior to their separation onto conjugate plates. The local scale of our study area allows us isolate this abandoned magmatic system and investigate the processes controlling its formation. We demonstrate that during SDR emplacement, rift-jumps of this scale result from interactions between separate magmatic systems that are segmented along-strike. The resulting models have a significant impact on our understanding of magmatic processes at the critical point of continental break-up.

2. Geological Setting

The West African magma-rich margin extends between the Walvis Ridge in the north and the Cape Segment Boundary in the south (Austin and Uchupi, 1982; Franke, 2013; Gladczenko et al., 1997; Koopmann et al., 2013; Light et al., 1993). It contains several sedimentary basins, the southernmost and largest being the Orange Basin (Séranne and Anka, 2005). The depocentre (Fig. 1) is located offshore South Africa and Namibia and trends NNW-SSE between 34° and 29°S, having an approximate length of 600 km. To the north it is bounded by the Luderitz Basin, and to the south by the Agulhas-Falkland Fracture Zone.

The rift geometry of the Orange Basin is considered to be an interplay between the regional extension associated with Gondwana break-up in the Late Jurassic, which commonly reactivated pre-existing crustal lineaments (Clemson et al., 1997; Gladczenko et al., 1997; Mohammed et al., 2016; Paton et al., 2016), and Atlantic rifting that formed a series of NNW-SSE trending half-grabens (Fig. 2, Light et al., 1993; Clemson et al., 1997; Paton et al., 2016; Mohammed et al., 2016). These half-grabens are controlled by landward-dipping normal faults that may be similar to those observed of rifted margins worldwide (Clerc et al., 2016). The syn-rift stratigraphy is largely undrilled, however, wells within the South African Orange Basin reveal that the half-grabens contain continental sandstones (alluvial and fluvial), lacustrine shales and basic volcanics (Gerrard and Smith, 1982; Jungslager, 1999). Above the syn-rift succession, a wide belt of SDRs is observed (Fig. 2), which is indicative of the transition from continental rifting to seafloor spreading (Fig. 2**,** Paton et al., 2016). Several wells within the Namibian Orange Basin sampled the landward edge of the SDRs (Wickens and McLachlan, 1990). These showed that the SDRs consist of basalts interbedded with aeolian and fluvial sandstones (Mohammed et al., 2016), indicating subaerial emplacement. The SDRs in the Orange Basin form part of the continuous c. 1600 km long SDR-belt extending northward to the Walvis Ridge (Gladczenko et al., 1997; Koopmann et al., 2013; McDermott et al., 2015). Regionally, a dominantly volcanic lithology of the SDRs is indicated by numerous seismic refraction profiles and potential field studies (Collier et al., 2017; Corner et al., 2002; Hirsch et al., 2009; Koopmann et al., 2014).

In the Orange Basin, continental breakup was diachronous and became younger towards the north, as is constrained by the occurrence of the M9-M4 seafloor spreading lineations, all of which occur within the Hauterivian (Collier et al., 2017). These seafloor spreading lineations occur within the unequivocal oceanic crust located seawards of the SDRs (Collier et al., 2017), and hence are not subject to the uncertainties associated with interpreting magnetic lineations in areas of ambiguous crustal type.

Following breakup the margin began to subside thermally, and open marine conditions were established during the Barremian-Aptian (Paton et al., 2008). Deposition continues to the present day, with the marine post-rift sediments reaching a current maximum thickness of 5.6 km (Dalton et al., 2016).

3. Study area and data

The study area is located in the South African Orange Basin (Fig. 1) and extends for approximately 100 km along strike. The primary 2D seismic reflection profile survey used in this study, which was acquired by Spectrum, was SPOB12 and images the entire continent-ocean transition across the margin. Dip lines trend NE-SW and are typically spaced at 30 km (Fig. 1a). The seismic data were recorded on a

10,050 m streamer containing 804 channels with receiver groups spaced at 12.5 m. The source was towed at 8 m depth and a shot interval of 25 m was used. Given the shot-receiver geometry, the maximum common midpoint gather (CMP) fold is 201 with CMPs being located every 6.25 m. Recording time was 10 s with a sample interval of 2 ms. The seismic data were pre-stack-time-migrated and pre-stack-depth-migrated, although additionally the raw gathers have been used to estimate seismic velocity.

A second seismic survey, K2002, was used to correlate horizons between the widely spaced SPOB12 lines (Fig. 1b). This survey had a recording time of 7 s and does not extend across the entire continent-ocean transition.

Seismic profiles are displayed with a blue reflection (positive) marking a downward increase in acoustic impedance, whereas red reflections (negative) mark a downward impedance decrease.

4 Seismic Interpretation

4.1 Methods

The seismic units mapped in the study area have neither been penetrated by boreholes nor extensively mapped in seismic data. Hence crucial to this study was the differentiation of normal oceanic crust and SDRs, and then the identification of several packages within the continent-ocean transition.

Across the study area the oceanic crust, SDRs and associated volcanic packages are separated from the post-rift succession by a high-amplitude positive reflector (Fig. 3). Previous studies have referred to this reflector as the break-up unconformity (Franke, 2013; Gerrard and Smith, 1982). We find this term unsuitable as many of the SDRs were likely emplaced as the uppermost part of thickened oceanic crust (Hinz, 1981; McDermott et al., 2015; Mutter et al., 1982; Paton et al., 2017), and hence break-up of the continental lithosphere pre-dates the occurrence of this unconformity. Instead of the ‘break-up unconformity’ we refer to this reflector as 6At1, which is in accordance with regional sequence stratigraphic models (Muntingh and Brown, 1993).

The age of the volcanics underlying 6At1 are uncertain. In comparison to other magmatic margins, e.g. the Vøring Plateau (Mutter et al., 1982) or the SE Greenland margin (Larsen and Saunders, 1998), the volcanics mapped here are considered to have been emplaced across a relatively short period of time (e.g. 2-4 Myrs; Koopmann et al., 2013) prior to the onset of the first normal oceanic crust in the Late Hauterivian (Collier et al., 2017).

Within this tectono-stratigrapic framework we apply a seismic characterisation technique that uses changes in seismic facies (Planke et al., 2000) to differentiate between the SDRs and normal oceanic crust. Packages within the Hauterivian volcanics were then defined through mapping and correlating changes in reflector configuration (Mitchum et al., 1977).

4.1.1 Identification of normal oceanic crust

Across the SW of the study area, the crust underlying the post-rift has a characteristic seismic character (Fig. 3, Fig. 4). The base of the post-rift is located at depths of 6.5-6.9 s TWTT and is defined by a high amplitude positive reflector which is underlain by 0.2-0.3 s TWTT of chaotic reflectors with moderate to low amplitudes. Beneath this layer is a zone of seismic transparency with a TWTT thickness of 0.6-0.8 s TWTT (Fig. 3a). The lower crust contains high amplitude reflectors with very variable dip directions, varying from landward-dipping, to near-horizontal, to seaward-dipping

(Fig. 3a). This zone of reflectivity is underlain by a band of near-horizontal high-amplitude reflectors (Fig. 3a).

This seismic character is consistent with examples of high-magma-supply oceanic crust worldwide (Bécel et al., 2015; Ranero et al., 1997; Reston et al., 1999) and is interpreted as such. In these settings oceanic crust typically conforms to the Penrose model of basalts, dolerite dykes and lower crustal gabbros (Penrose field conference on ophiolites [Geotimes, v. 17, p. 24–25]).

The high amplitude top-basement reflection in Fig. 3 and Fig. 4 represents the basalt-sediment interface and the 0.2-0.3 s TWTT thick zone of chaotic reflections underlying it are likely to correspond to the reflectivity within pillow basalts and sheet flows. The zone of seismic transparency lying directly beneath this represents sheeted dykes and the uppermost gabbros (Fig. 3b). In the lower crust, the high amplitude reflectors observed here are similar to the intra-gabbroic reflectors (Fig. 3b) imaged in oceanic crust worldwide (Bécel et al., 2015; Ranero et al., 1997; Reston et al., 1999). In seismic reflection data the oceanic Moho is often imaged as a diffuse zone of high amplitude reflectivity (Mutter and Carton, 2013), which is how we interpret the band of near horizontal reflectors located at c. 9.3 s TWTT (Fig. 3b).

4.1.2 Identification and mapping of SDRs

SDRs were identified by their characteristic geometry (Mutter et al., 1982), whereby, all reflectors dip seawards, have a convex-up geometry, and diverge downdip into a zone of chaotic seismic imaging (e.g. Fig. 3). Mapping the width of the SDR belt is commonly used to constrain the variations in the amount of volcanics emplaced along-strike in this region (Koopmann et al., 2014, 2013). In this study, the width of the SDR belt has been calculated by measuring the horizontal distance from the downdip termination of the first (oldest, and landward-most) to the last (youngest, and seaward-most) SDR (Fig. 3).

4.2 Basin architecture

Using the classifications outlined above, SDRs and oceanic crust were mapped across the study area, and variations from these two seismic units were identified and described.

Oceanic crust is located across the SW of the study area (Fig. 3, Fig. 4), landwards, this oceanic crust transitions into a belt of SDRs, within which all reflectors dip seawards with a downdip divergence (Fig. 3, Fig. 4). Pre-stack depth migrated profiles, which show the depth-converted geometry of the SDRs, indicate that individual reflectors have convex-up with dips ranging from 5-20° (Fig. 3c). In addition to their diagnostic geometry, the SDRs have a distinctive seismic character comprising strong amplitude variations along individual SDRs (Fig. 3a). Occasional high amplitude saucer shaped reflectors are also observed (Fig. 3b). These are broadly concordant with the SDRs with discordance occurring near the saucer tips and correspond to localised sill intrusions (e.g. Planke et al., 2005).

Underlying the SDRs are densely spaced landward-dipping reflectors which have variable amplitudes (Figs 3a and 4b). Where these two sets of reflectors intersect, the landward dipping reflectors cross-cut the SDRs, although no intra-SDR offsets are observed (Fig. 4b). We interpret these landward-dipping reflectors as dykes which were emplaced at the same time as the SDRs. This interpretation is supported by the lack of offsets observed where the landward-dipping reflectors cross-cut the SDRs, which indicates that they are not faults. The seismic character of this set of reflectors is also similar to that of dyke swarms imaged in the North Sea basin (Phillips et al., 2018) and the Vøring margin (Abdelmalak et al., 2015).

In the south of the study area the SDR belt is very wide (e.g. 88 km in Fig. 1b, Fig. 1b), and consists of a continuous succession in which no major unconformities are present. 30 km landward of the SDR/oceanic crust interface the quality of the SDRs imaging is reduced by an overlying volcanic complex consisting of mounded, rugose high amplitude reflectors (these are labelled as ‘post-SDR volcanics’ in Fig. 3b). Disrupted SDRs can be identified beneath this volcanic complex, hence it was either emplaced during the emplacement of the latest SDRs (i.e. during the emplacement of those SDRs located seawards of the mound) or during the earliest post-rift. The occurrence of this structure is limited to this seismic line.

The >80 km SDR belt width in the south (Fig. 3) is in noticeable contrast to a section 30 km towards the north-west (Fig. 4) in which the width is 26 km. This, therefore, corresponds to a significant narrowing of the SDR belt by ~ 54 km over 30 km along-strike (Fig. 1b).

This substantial narrowing of the SDR belt towards the north-west coincides with the presence of a previously unrecognised seismic package (orange package in Fig. 4b) that only occurs in the north of the study area and underlies the SDRs. This additional package is thickest in a central axial zone (labelled Axis 1.1), reaching a thickness of c. 0.85 s TWTT (c. 2400 m thick based on the interval velocities shown in Supp. Fig. 2b), and thins in a near symmetrical geometry both landwards and seawards (Fig. 4b). A fanning of dips is observed within the package and stratal thinning is accommodated by onlap towards the mini-basin flanks. The base of the package is a high amplitude onlap surface, whilst its top is defined as the reflector above which there is no prominent thickening into the axial trough. Slightly east of the central axis, the package is cross-cut by a near vertical zone of disruption; reflectors can be correlated across this zone without any offset and hence it cannot be interpreted as a major fault. The width of the package has been plotted onto the margin domain map in Fig. 1b, and its occurrence directly correlates with the northward narrowing of the SDR wedge. Given the geometry of this package we name it the Laterally Confined Volcanic Succession, or LCVS. Its volcanic lithology has been validated through seismic velocity analysis (see Supplementary Material).

Directly underlying the LCVS are two wedges of reflectors that both thicken downdip into an axial zone of chaotic imaging (Wedges 1 and 2 in Fig. 4b). Wedge 1 contains dominantly landward dipping reflectors, whilst Wedge 2 consists of reflectors which all dip seawards and are identical to SDRs. Wedge 1 is less well imaged than its seaward dipping counterpart, which is likely to be a result of the locally thicker overburden.

Our observations demonstrate that the SDR belt narrows northwards across the study area, and that this narrowing is accompanied by the occurrence of a new package, the LCVS. In order to understand the lithology, evolution, and significance of the LCVS we now consider the temporal and spatial relationship between the SDRs and the LCVS.

4.3 Relationship between the LCVS and the SDRs

As noted previously, the SDR belt narrows from 88 km to 26 km across the relatively short distance of 30 km (Fig. 1b), and this narrowing is accompanied by the occurrence of the LCVS. In order to investigate the temporal and spatial relationship between the LCVS and the SDRs, three reflectors (R1, R2 and R3), have been correlated across the dataset (these reflectors are shown in figures 3b and 4b). This allows us to identify three distinct stage of margin evolution: stage a which is bounded by R1 and R2; stage b which is bounded by R2 and R3; and stage c which consists of the SDRs overlying R3. In this section we summarise the observations for each of these stages, and in a subsequent section (Section 5) we propose a model for their evolution.

4.3.1 Stage a (R1-R2)

The package bounded by R1 and R2 allow us to investigate the along-strike relationship between the LCVS and SDRs (Fig. 5). In the north of the study area, R1 and R2 correspond to the top and the base of the LCVS respectively (seismic line A, Fig. 5). The R1-R2 isochron (Fig. 6a) demonstrates that the LCVS trends NNW-SSE, is c. 50 km long and up to 30 km wide. The thickness of the LCVS is greatest within a NNW-SSE trending axial zone (Axis 1.1 in Fig. 6b), although this also shows along-strike thickness variations. Seismic line A (Fig. 5) is located through the thickest part of the LCVS (Fig. 6a), with vertical thickness reaching 0.85 s TWTT in the axial zone. Away from this axial zone the landward and seaward stratal thinning is near symmetrical.

Seismic line B (Fig. 5) is located some 15 km SE of seismic line A, and is positioned over the southernmost flank of the LCVS (Fig. 6a). Here the thickness of the axial zone reaches 0.32 s TWTT (c. 0.9 km; Supp. Fig. 2b) and, while stratal thinning does occur both landwards and seawards of this zone, it is not as pronounced as in line A. Located in the south of the study area, seismic line C (Fig. 5) shows that reflections R1 and R2 bound a package of SDRs and there is no LCVS present. Close to their down-dip termination this package reaches a maximum thickness of 0.54 s TWTT (c. 1.5 km, Fig. 5). The R1-R2 isochron map (Fig. 6a) illustrates that this lateral transition, from LCVS to SDRs, occurs through the progressive diminishment of the former and the development of the latter. No seismically resolvable faults are present in this transition zone. Therefore, it is through this gradual lateral transition that the SDR belt shows southward widening. Also evident from the isochron (Fig. 6a) is that the downdip termination of R1-R2 bounded SDRs, named Axis 1.2 (Fig. 6a, and Fig. 5), is offset ≥10 km SW from the LCVS axial zone (Axis 1.1 in Fig. 6a).

Mapping of the package bounded by R1-R2 has demonstrated that during stage a, the LCVS was developing in the north of the study area, whilst SDRs were developing in the south.

4.3.2 Stage b (R2-R3)

It has been demonstrated that the nature of R2 varies across the study area – in the north it defines the top of the LCVS (lines a and b in Fig. 5), whilst in the south it is an intra-SDR belt reflector (line c in Fig. 5). The package bounded by reflectors R2 and R3 also varies structurally across the area. In the south (Fig. 3b), this package consists of a wedge of SDRs which conformably overlie the stage a SDRs. Meanwhile, in the north of the study area this package is reduced in thickness and differs geometrically from SDRs (Fig. 4b). Whereas SDRs show continuous downdip divergence, here thickness variations are limited to the updip pinchout of the package and downdip from this area stratigraphic thickness appears relatively constant (Fig. 4b).

4.3.3 Stage c (post-R3 SDRs)

Stage c is characterised by the occurrence of SDRs across the study area. These SDRs form a continuous succession from R3 to the transitional boundary between the SDRs and normal oceanic crust (Fig 3b, Fig. 4b). An isochron of the stage c SDRs shows thickness variations across the study area (Fig. 6b). The top of the isochron is defined as 6At1 (Fig. 3a, Fig. 4a) and the base is defined as composite horizon consisting of R3 and the SDR downdip terminations (this composite horizon is shown in figures 3a and 4a). The isochron (Fig. 6b) demonstrates that continuous

SW thickening occurs from the updip pinchout of the succession to the first downdip SDR termination, which is labelled as Axis 2 on the isochron (Fig. 6b) and the corresponding seismic sections (Fig.4b, Fig. 3b). Axis 2 trends NNW-SSE across the study area (Fig. 6b), and although several kinks are observed we interpret this as a continuous axis (as opposed to the two axes being present in Stage 1). This interpretation is based on stage c being defined by the development of SDRs across the study area, whilst stage a was defined by the development of SDRs and the LCVS. Immediately SW of Axis 2, thickness variations are less pronounced until the SDR belt begins thinning SW towards the location of the first ‘normal’ oceanic crust (labelled in Fig. 6b).

4.3.4 Comparison between features from stages a to c

Axes 1.1 and 1.2 were defined in relation to stage a, whilst Axis 2 was defined in relation to the stage c. As will be shown in the discussion, these axes can be used to infer the 3D evolution of the SDRs and the LCVS, as such the spatial relationships between them is important. All of the axes trend approximately NNW-SSE and are margin-parallel, however the offsets between the stage a and stage c axes vary. In the north, where the LCVS is present, there is an offset of ≤25 km between Axis 1.1 and Axis 2 (Fig 6b, Fig 4b). Meanwhile in the south of the study area, where axes 1.2 and 2 are separated by a continuous succession of SDRs, there is an offset of c. 12 km (Fig. 3b, Fig. 6b).

5. Discussion

5.1 Formation of the Laterally Confined Volcanic Sequence

During emplacement, the lava flows that became SDRs were emplaced above an axial magma-source (Larsen and Saunders, 1998; Mutter et al., 1982; Paton et al., 2017; Quirk et al., 2014). Continued plate separation resulted in the accretion of more magmatic material in this axial zone which forced older lava flows to be transported away from the axis and to be progressively rotated to their present dips. Above the axial magma-chamber the SDRs were fed by intrusions, and this SDR/intrusive contact is preserved today at their down-dip terminations (Paton et al., 2017). In seismic reflection data, these down-dip terminations are defined by rapid dimming into a zone of chaotic seismic imaging where occasional landward dipping reflectors are present. In terms of seismic character, this is similar to the axial zone that separates the landward and seaward diverging wedges that are observed beneath the LCVS (wedges 1 and 2 in Fig. 4b). Based upon the similarities between geometry, seismic character (Fig. 4b) and bulk lithology (Supp. Fig. 1; Supp. Fig. 2), we interpret the package underlying the LCVS as being formed by the same processes as SDRs. In other words, these two wedges of volcanics were fed from an axial magmatic spreading centre (Fig. 7a, i), which today is preserved as the axial zone of chaotic imaging (Fig. 4b).

The LCVS is unfaulted and onlaps the underlying volcanic package (Fig. 4B), and the seismic velocities indicate that it also comprises mainly volcanics (Supp. Fig. 1; Supp. Fig. 2). The axial zone, in which this package is thickest, overlies the magma source that fed the underlying volcanics (Axis 1.1 in Fig. 4b). This observation, in addition to axial disruptions within the LCVS, strongly suggests that it was also sourced from this underlying magma-source (Fig. 7a, i). As mentioned previously, the volcanics directly underlying the LCVS were emplaced via the same mechanism as SDRs. Meanwhile, the reflectors within the LCVS onlap against these underlying volcanics, and are often confined to a mini-basin. The structural confinement indicates that extrusion rate was now less than the subsidence rate, with this subsidence being driven by either waning magma-supply (Mutter et al., 1982) or flexure driven by underlying intrusives (Buck, 2017; Corti et al., 2015). The unfaulted nature of the LCVS is important as it provides insights into the processes controlling subsidence on magma-rich margins. The relative roles of faulting (Clerc et al., 2015; Geoffroy et al., 2015; Quirk et al., 2014) and magmatic loading (Buck, 2017; Corti et al., 2015; Paton et al., 2017) in generating the dips recorded by SDRs are disputed. The LCVS provides an unambiguous example of subsidence being generated without normal faulting. Hence the architecture of this package supports models of SDR formation in which subsidence is generated via the magmatic loading of thin and weak crust (Buck, 2017; Corti et al., 2015; Paton et al., 2017).

The LCVS is overlain by SDRs (Fig. 4b), the emplacement of which indicates the eventual abandonment of the magmatic zone feeding the LCVS and the establishment of a new magmatic zone ≤25 km to the SW (Fig. 7b, i). This new magmatic zone remained active throughout the remainder of the breakup process, resulting in an SDR belt with a width of 26 km. Continental breakup results in a wedge of SDRs being preserved on each conjugate margin. Hence the wedge of SDRs conjugate to that shown in Fig. 4B is located offshore Argentina (Franke et al., 2007; Koopmann et al., 2014; Paton et al., 2017). The width of the Argentinian SDR belt varies along-strike and there are examples where the SDRs have similar dimensions to those located seawards of the LCVS (Franke et al., 2007), however further work would be needed to validate this.

Our model implies that the LCVS and the underlying package formed via the same mechanism as SDRs, however, the subsequent jump in the location of magmatism resulted in this early magmatic spreading system being preserved in its entirety (Fig. 7a, i). The majority of previous studies have implied that flood basalts erupted during the rift-drift transition are sourced from a single axial magma-system, which results in wide belts of SDRs (Mutter et al., 1982; Paton et al., 2017; Quirk et al., 2014). However here we demonstrate that this magma-source can jump in space and time. Whilst the possibility of ‘rift-jumps’ disrupting the SDR belt has been suggested by previous authors (Buck, 2017; Pindell et al., 2014), this is the first unambiguous example of one such jump in seismic reflection data.

5.2 What drives rift-jumps during SDR formation?

It has recently been suggested that a series of rift-jumps can occur during this SDR emplacement (Buck, 2017). This model is supported by the presence of unconformities within SDR belts, indicating episodic emplacement (Franke et al., 2007; Koopmann et al., 2013). This is in contrast to previous studies, which suggest that SDR emplacement is, to a large extent, a continuous process (Mutter et al., 1982; Paton et al., 2017; Quirk et al., 2014).

We observe that both models are applicable to different parts of the study area - in the south of the area the SDR belt is 88 km wide (Fig. 3) and its structural uniformity indicates that the SDRs were emplaced above, and transported away from, an axial magma source that remained spatially fixed (Fig. 7a, ii, Fig. 7b, ii). Meanwhile, in the north of the study area (Fig. 4) the magma-source did not remain fixed but jumped, leading to the preservation of the LCVS (Fig. 7a, i; Fig. 7b, i).

From these results it is evident that rift-jumps of the scale recorded here are local, not regional, features. Through assessing the 3D evolution of the study area we can assess what is driving a rift-jump in the north, and continuous SDR emplacement in the south. It is suggested that the rift-jump observed has fundamental implications for SDR emplacement.

A three-stage model, stage a–c, is presented to demonstrate the 3D tectono-magmatic evolution of the study area (Fig. 7). During stage a, the LCVS and underlying package were emplaced contemporaneously with SDRs in the south (Fig. 5). The axial zone, Axis 1.1 (Fig. 6a), of the LCVS directly overlies the magma-chamber that fed this and the underlying package. The contemporary SDRs being emplaced to the south were fed from a magma-chamber located beneath their present-day down-dip terminations (Axis 1.2 in Fig. 6a). Therefore, at this stage of the breakup process, magmatism was partitioned along-strike into two segments, which were laterally offset by c. 15 km (Fig. 7a, iii). Although one such feature is not imaged in these seismic reflection data, it is possible that two these segments were separated by a transfer zone with dextral offset (Fig. 7a, iii).

During stage b, SDR emplacement continued in the south of the study area, as is evident from a thick wedge of volcanics developing during this time (Fig. 3b). These SDRs conformably overlie those emplaced during stage a, indicating that locally, SDR emplacement was continuous from one stage to the next (Fig. 7b, ii). The north of the study area, meanwhile, is characterised by relatively little active magmatism. The magmatic zone feeding the LCVS was abandoned, and a package with relatively constant thickness was emplaced (Fig. 7b, i) conformably on top of the LCVS. This package is interpreted as volcanics that were passively infilling remnant topography (Fig. 7b, i).

Stage c is defined by SDR emplacement across the study area, as is shown by SDRs being present in seismic lines both in the north (Fig. 4b) and the south (Fig. 3b). These SDRs are relatively uniform in terms of along-strike thickness and width (Fig. 6b). In section 4, Axis 2 was defined as the downdip termination of the oldest SDR within this package (i.e. the base of the package), this axis represents the trend of the magmatic zone which was established during this stage. Axis 2 trends NNW-SSE and only small kinks in this trend are present. This, in addition to the along-strike uniformity of this package, indicates that the stage c SDRs were emplaced from a laterally continuous axial zone that extended across the study area(Fig. 7c, iii).

Our model suggests that from stage a to stage c there is a transition from a magmatic system that was segmented along-strike (Fig. 7a, iii), to one that was relatively continuous along-strike (Fig. 7c, iii). By comparing the magmatic axes defined for each of these stages, we can assess how this transition occurs. In the south of the study area, there is an offset of 12 km (Fig. 3b) between the stage a (Axis 1.2) and stage c (Axis 2) axes (Fig. 6b). As was discussed above, in this part of the study area, SDR emplacement appears to have been relatively continuous through time. Therefore the offset between axes 1.2 and 2 is explained by 12 km of SDR emplacement occurring between stages a and c (Fig. 7b, ii). However, in the north of the study area, the offset between the stage a (Axis 1.1) and stage c (Axis 2) axes cannot be explained by this mechanism. Rather, this offset results from a rift-jump of 25 km (Fig. 7c, i), resulting in the present-day preservation of the LCVS (Section 5.1). Therefore it is clear that this rift-jump records this transition from a laterally segmented, to an axially aligned magmatic system. The specific cause of the rift-jump can now be investigated.

It is notable that the laterally continuous magmatic system of stage c occurs along the same trend as that present in the south of the study area during both stages a and b (see maps in Fig. 7). This may imply that the southern magmatic system of stage a (axis 1.2) was propagating northwards (maps in Fig. 7). If this was the case then the localisation of strain on the propagating magmatic zone may have resulted in the abandonment of the LCVS. In two-dimensions, this process would be recorded by the rift-jump evident in seismic sections through the north of the study area. This mechanism for LCVS formation is consistent with observations from overlapping seafloor spreading centres – where one spreading segment can be ‘decapitated’ by the propagation of the other (Macdonald et al., 1998). The northward propagation of individual magmatic segments is also consistent with the regional opening direction of the South Atlantic (Jackson et al., 2000), although such northward opening has been previously unrecognised at this scale. We suggest that stage b, where active magmatism was occurring in the south but not in the north, marks the stage where northward propagation of the southward segment coincided with the abandonment of that feeding the LCVS.

This process provides a mechanism for the rift-jumps of similar magnitude that have recently been modelled as occurring during SDR emplacement (Buck, 2017). These models use rift-jumps to explain the 2D structure of magma-rich margins, however our results show that these events may result from 3D interactions between separate magmatic segments. Whilst our results suggest that these processes act on a local scale, they will necessarily affect the interpretation of isolated seismic reflection lines.

5.3 Rift-jumps and margin segmentation

The Orange Basin is divided along strike into a series of segments separated by transfer zones with a spacing of >100 km (Clemson et al., 1997; Koopmann et al., 2013). These transfer zones can be either strike-slip faults or basement highs (Clemson et al., 1997). The data shown in this study are located between two such segment boundaries, the Namaqua Segment Boundary to the north, and the Cape Segment Boundary to the south (Fig. 1, Clemson et al., 1997; Koopmann et al., 2013). We have demonstrated that during the emplacement of the LCVS the basin was segmented along strike into a series of laterally offset magmatic centres (stage a, Fig. 7). These magmatic centres were laterally offset 15 km from one another, and it is possible that a transfer zone (Fig. 7, stage c) separated them. This segmentation occurs between the regionally spaced segment boundaries described in previous studies (Clemson et al., 1997; Koopmann et al., 2013), and hence represents an order of segmentation that has not been previously recognised on magma-rich margins. Furthermore, in contrast to the regional segmentation previously described, this smaller-scale segmentation was not present throughout the entire breakup process: it was present during the emplacement of the LCVS (stage a, Fig. 7), but was erased by a subsequent rift jump (stage c, Fig. 7). We have suggested that the mechanism driving this rift-jump was the northward propagation (section 5.2) of an adjacent magmatic segment. However, regardless of the mechanism, it is notable that the system evolved from being segmented along-strike (stage a) to relatively continuous along-strike (stage c). We suggest that rift-jumps such as that interpreted here, may occur to accommodate the formation of a laterally continuous magmatic spreading zone. As such, this model may be applicable to the generic process of SDR emplacement. Specifically, it offers a mechanism for the occurrence of the discrete wedges of SDRs observed on 2D seismic reflection profiles across the South Atlantic magma-rich margins (Franke et al., 2010; Koopmann et al., 2013). These wedges are separated by unconformities, and may record a series of small (<10 km) rift-jumps as the system becomes progressively less structurally segmented along-strike.

6. Conclusions

SDRs have become diagnostic features of magma-rich margins globally. In this study we identify a new volcanic package, the Laterally Confined Volcanic Succession (LCVS), which is also present in these settings. The LCVS was produced by a rift-jump during SDR emplacement, and provides an example of SDR-geometry prior to plate separation.

Previous models have suggested that rift-jumps may be common during the formation of SDRs, however the driving mechanism remained uncertain. The 3D evolution of the magmatic system in the Orange Basin indicates that such rift-jumps occur to allow strain localisation on a continuous axial magmatic zone. This results in the abandonment of the structural segmentation present earlier in the breakup process. We suggest that this process may be fundamental in the development of an incipient spreading centre, and that such magmatic-driven rift-jumps should be observable on other magma-rich margins.

Acknowledgements

We would like to thank Spectrum for providing the seismic data used in this study, and for permission to publish. We are also grateful to Schlumberger and Halliburton for providing the University of Leeds with academic software licenses. James Norcliffe was supported by a PhD scholarship funded by an industry consortium.

References

Abdelmalak, M.M., Andersen, T.B., Planke, S., Faleide, J.I., Corfu, F., Tegner, C., Shephard, G.E., Zastrozhnov, D., Myklebust, R., 2015. The ocean-continent transition in the mid-Norwegian margin: Insight from seismic data and an onshore Caledonian field analogue. Geology 43, G37086.1. https://doi.org/10.1130/G37086.1

Austin, J.A.J., Uchupi, E., 1982. Continental-Oceanic Crustal Transition Off Southwest Africa. Am. Assoc. Pet. Geol. Bull. 66. https://doi.org/10.1306/03B5A79B-16D1-11D7-8645000102C1865D

Bécel, A., Shillington, D.J., Nedimović, M.R., Webb, S.C., Kuehn, H., 2015. Origin of dipping structures in fast-spreading oceanic lower crust offshore Alaska imaged by multichannel seismic data. Earth Planet. Sci. Lett. 424, 26–37. https://doi.org/10.1016/j.epsl.2015.05.016

Buck, W.R., 2017. The role of magmatic loads and rift jumps in generating seaward dipping reflectors on volcanic rifted margins. Earth Planet. Sci. Lett. 466, 62–69. https://doi.org/10.1016/j.epsl.2017.02.041

Clemson, J., Cartwright, J., Booth, J., 1997. Structural segmentation and the influence of basement structure on the Namibian passive margin. J. Geol. Soc. London. 154, 477–482. https://doi.org/10.1144/gsjgs.154.3.0477

Clerc, C., Jolivet, L., Ringenbach, J.-C., 2015. Ductile extensional shear zones in the lower crust of a passive margin. Earth Planet. Sci. Lett. 431, 1–7. https://doi.org/10.1016/j.epsl.2015.08.038

Clerc, C., Ringenbach, J.C., Jolivet, L., Ballard, J.F., 2016. Rifted margins: Ductile deformation, boudinage, continentward-dipping normal faults and the role of the weak lower crust. Gondwana Res. https://doi.org/10.1016/j.gr.2017.04.030

Collier, J.S., McDermott, C., Warner, G., Gyori, N., Schnabel, M., McDermott, K., Horn, B.W., 2017. New constraints on the age and style of continental breakup in the South Atlantic from magnetic anomaly data. Earth Planet. Sci. Lett. 477, 27–40. https://doi.org/10.1016/j.epsl.2017.08.007

Corner, B., Cartwright, J., Swart, R., 2002. Volcanic passive margin of Namibia: A potential fields perspective. Geol. Soc. Am. Spec. Pap. 362, 203–220. https://doi.org/10.1130/0-8137-2362-0.203

Corti, G., Agostini, a., Keir, D., Van Wijk, J., Bastow, I.D., Ranalli, G., 2015. Magma-induced axial subsidence during final-stage rifting: Implications for the development of seaward-dipping reflectors. Geosphere 11, 563–571. https://doi.org/10.1130/GES01076.1

Dalton, T.J.S., Paton, D. a, Needham, D.T., 2016. Influence of mechanical stratigraphy on multi-layer gravity collapse structures: insights from the Orange Basin, South Africa. Geol. Soc. London, Spec. Publ. 438. https://doi.org/10.1144/SP438.4

Eldholm, O., Grue, K., 1994. North Atlantic volcanic margins : Dimensions and production rates a volume of flood basalts a mean eruption rate of the basalts were emplaced within volume in a mean crustal accretion rate. J. Geophys. Res. 99, 2955–2968.

Franke, D., 2013. Rifting, lithosphere breakup and volcanism: Comparison of magma-poor and volcanic rifted margins. Mar. Pet. Geol. 43, 63–87. https://doi.org/10.1016/j.marpetgeo.2012.11.003

Franke, D., Ladage, S., Schnabel, M., Schreckenberger, B., Reichert, C., Hinz, K., Paterlini, M., de Abelleyra, J., Siciliano, M., 2010. Birth of a volcanic margin off Argentina, South Atlantic. Geochemistry, Geophys. Geosystems 11, n/a-n/a. https://doi.org/10.1029/2009GC002715

Franke, D., Neben, S., Ladage, S., Schreckenberger, B., Hinz, K., 2007. Margin segmentation and volcano-tectonic architecture along the volcanic margin off Argentina/Uruguay, South Atlantic. Mar. Geol. 244, 46–67. https://doi.org/10.1016/j.margeo.2007.06.009

Geoffroy, L., Burov, E.B., Werner, P., 2015. Volcanic passive margins: another way to break up continents. Sci. Rep. 5, 14828. https://doi.org/10.1038/srep14828

Gerrard, I., Smith, G., 1982. Post-Paleozoic succession and structure of the southwestern African continental margin. Stud. Cont. margin Geol. AAPG Mem.

Gladczenko, T.P., Hinz, K., Eldholm, O., Meyer, H., Neben, S., Skogseid, J., 1997. South Atlantic volcanic margins. J. Geol. Soc. London. 154, 465–470. https://doi.org/10.1144/gsjgs.154.3.0465

Hey, R., 1977. A new class of “pseudofaults” and their bearing on plate tectonics: A propagating rift model. Earth Planet. Sci. Lett. 37, 321–325. https://doi.org/10.1016/0012-821X(77)90177-7

Hinz, K., 1981. A hypothesis on the terrestrial catastrophes wedges of very thick oceanward dipping layers beneath passive continental margind — their origin and paleonevironmental significance. Geol. Jahrb. R. E.

Hirsch, K.K., Bauer, K., Scheck-Wenderoth, M., 2009. Deep structure of the western South African passive margin - Results of a combined approach of seismic, gravity and isostatic investigations. Tectonophysics 470, 57–70. https://doi.org/10.1016/j.tecto.2008.04.028

Jackson, M.P.., Cramez, C., Fonck, J.-M., 2000. Role of subaerial volcanic rocks and mantle plumes in creation of South Atlantic margins: implications for salt tectonics and source rocks. Mar. Pet. Geol. 17, 477–498. https://doi.org/10.1016/S0264-8172(00)00006-4

Jungslager, E.H.A., 1999. Petroleum habitats of the Atlantic margin of South Africa. Geol. Soc. London, Spec. Publ. 153, 153–168. https://doi.org/10.1144/GSL.SP.1999.153.01.10

Koopmann, H., Franke, D., Schreckenberger, B., Schulz, H., Hartwig, A., Stollhofen, H., di Primio, R., 2013. Segmentation and volcano-tectonic characteristics along the SW African continental margin, South Atlantic, as derived from multichannel seismic and potential field data. Mar. Pet. Geol. 50, 22–39. https://doi.org/10.1016/j.marpetgeo.2013.10.016

Koopmann, H., Schreckenberger, B., Franke, D., Becker, K., Schnabel, M., 2014. The late rifting phase and continental break-up of the southern South Atlantic: the mode and timing of volcanic rifting and formation of earliest oceanic crust. Geol. Soc. London, Spec. Publ. 420. https://doi.org/10.1144/SP420.2

Larsen, H.C., Saunders, A.D., 1998. 41. Tectonism and volcanism at the southeast Greenland rifted margin: a record of plume impact and later continental rupture. Proc. Ocean Drill. Program, Sci. Results 152.

Light, M.P.., Maslanyj, M.P., Greenwood, R.J., Banks, N.L., 1993. Seismic sequence stratigraphy and tectonics offshore Namibia. Geol. Soc. London Spec. Publ. 71, 163–191.

Manatschal, G., 2004. New models for evolution of magma-poor rifted margins based on a review of data and concepts from West Iberia and the Alps. Int. J.

Earth Sci. https://doi.org/10.1007/s00531-004-0394-7

McDermott, K., Gillbard, E., Clarke, N., 2015. From Basalt to Skeletons – the 200 million-year history of the Namibian margin uncovered by new seismic data. First Break 33, 77–85.

Mitchum Jr., R.M., Vail, P.R., Sangree, J.B., 1977. Seismic stratigraphy and global changes of sea level, Part six: stratigraphic interpretation of seismic reflection patterns in depositional sequences. Seism. Stratigr. — Appl. to Hydrocarb. Explor. 165, 117–134. https://doi.org/10.1038/272400a0

Mittelstaedt, E., Ito, G., Van Hunen, J., 2011. Repeat ridge jumps associated with plume-ridge interaction, melt transport, and ridge migration. J. Geophys. Res. Solid Earth 116, 1–20. https://doi.org/10.1029/2010JB007504

Mohammed, M., Paton, D., Collier, R.E.L., Hodgson, N., 2016. Interaction of crustal heterogeneity and lithospheric processes in determining passive margin architecture on the southern Namibian margin. Geol. Soc. London, Spec. Publ. 438.

Muntingh, A., Brown, L.F., 1993. Sequence stratigraphy of Petroleum Plays, Post-Rift Cretaceous Rocks (Lower Aptian to Upper Maastrchtian), Orange Basin, Western Offshore, South Africa, in: Siliciclastic Sequence Stratigraphy. Recent Develepments and Apllications.

Mutter, J., Talwani, M., Stoffa, P., 1982. Origin of seaward-dipping reflectors in oceanic crust off the Norwegian margin by “subaerial sea-floor spreading.” Geology 10, 353–357.

Mutter, J.C., Carton, H.D., 2013. The mohorovicic discontinuity in ocean basins: Some observations from seismic data. Tectonophysics 609, 314–330.

https://doi.org/10.1016/j.tecto.2013.02.018

Paton, D. a., Pindell, J., McDermott, K., Bellingham, P., Horn, B., Repository, G.S.A.D., 2017. Evolution of seaward-dipping reflectors at the onset of oceanic crust formation at volcanic passive margins: Insights from the South Atlantic. Geology 45, G38706.1. https://doi.org/10.1130/G38706.1

Paton, D. a., van der Spuy, D., di Primio, R., Horsfield, B., 2008. Tectonically induced adjustment of passive-margin accommodation space; influence on the hydrocarbon potential of the Orange Basin, South Africa. Am. Assoc. Pet. Geol. Bull. 92, 589–609. https://doi.org/10.1306/12280707023

Paton, D. a, Mortimer, E.J., Hodgson, N., Van Der Spuy, D., 2016. The missing piece of the South Atlantic jigsaw - when continental break-up ignores crustal heterogeneity. Pet. Geosci. West Africa Margin, Geol. Soc. London, Spec. Publ. 438. https://doi.org/http://doi.org/10.1144/SP438.8

Péron-Pinvidic, G., Manatschal, G., 2008. The final rifting evolution at deep magma-poor passive margins from Iberia-Newfoundland: a new point of view. Int. J. Earth Sci. 98, 1581–1597. https://doi.org/10.1007/s00531-008-0337-9

Phillips, T.B., Magee, C., Jackson, C.A.L., Bell, R.E., 2018. Determining the three-dimensional geometry of a dike swarm and its impact on later rift geometry using seismic reflection data. Geology 46, 119–122. https://doi.org/10.1130/G39672.1

Pindell, J., Graham, R., Horn, B., 2014. Rapid outer marginal collapse at the rift to drift transition of passive margin evolution, with a Gulf of Mexico case study. Basin Res. 701–725. https://doi.org/10.1111/bre.12059

Planke, S., Eldholm, O., 1994. Seismic response and construction of seaward dipping wedges of flood basalts : Voring volcanic margin. J. Geophys. Res. Solid Earth 99, 9263–9278.

Planke, S., RASMUSSEN, T., REY, S.S., MYKLEBUST, R., 2005. Seismic characteristics and distribution of volcanic intrusions and hydrothermal vent complexes in the Vøring and Møre basins. Geol. Soc. London, Pet. Geol. Conf. Ser. 6, 833–844. https://doi.org/10.1144/0060833

Planke, S., Symonds, P.A., Alvestad, E., Skogseid, J., 2000. Seismic volcanostratigraphy of large-volume basaltic extrusive complexes on rifted margins. J. Geophys. Res. Solid Earth 105, 19335–19351. https://doi.org/10.1029/1999JB900005

Quirk, D.G., Shakerley, A., Howe, M.J., 2014. A mechanism for construction of volcanic rifted margins during continental breakup. Geology 42, 1079–1082. https://doi.org/10.1130/G35974.1

Ranero, C.R., Reston, T.J., Belykh, I., Gnibidenko, H., 1997. Reflective oceanic crust formed at a fast-spreading center in the Pacific. Geology 25, 499–502. https://doi.org/10.1130/0091-7613(1997)025<0499:ROCFAA>2.3.CO;2

Reston, T.J., Ranero, C.R., Belykh, I., 1999. The structure of Cretaceous oceanic crust of the NW Pacific: Constraints on processes at fast spreading centers. J. Geophys. Res. 104, 629. https://doi.org/10.1029/98JB02640

Séranne, M., Anka, Z., 2005. South Atlantic continental margins of Africa: A comparison of the tectonic vs climate interplay on the evolution of equatorial west Africa and SW Africa margins. J. African Earth Sci. 43, 283–300. https://doi.org/10.1016/j.jafrearsci.2005.07.010

White, R., McKenzie, D., 1989. Magmatism at rift zones: The generation of volcanic continental margins and flood basalts. J. Geophys. Res. 94, 7685. https://doi.org/10.1029/JB094iB06p07685

Wickens, H.D. V, McLachlan, I.R., 1990. The stratigraphy and seidmentology of the reservoir interval of the Kudu 9A-2 and 9A-3 boreholes. Commun. Geol. Surv. Namibia 6, 9–22.

Figure Captions

Fig. 1. a) Regional map showing the location of the Orange Basin, outlined in a red dashed line, in relation to Namibia and the Republic of South Africa (RSA). Seismic lines are also shown, with SPOB12 in black and K2002 in orange. The segment boundaries of Koopmann et al., 2013 are shown in as brown dashed lines. In a) the study area is shown a red box. b) Sketch map of the study area, showing the location of seismic lines and the width of the structural remains described in the text. Black dashed line show bathymetry (m below sea level).

Fig. 2. Representative cross-section through the Orange Basin, line location is shown in Fig. 1a. Figure demonstrates the structure of the syn-rift, SDRs and post-rift. Modified from Mohammed et al., 2016.

Fig. 3. a) PSTM seismic reflection line with a vertical exaggeration of 5:1, the line location is shown in Fig. 1b. The black dashed line demonstrated the base of the isochore shown in Fig. 6b. b) Seismic line shown in a) with interpretation, four packages of SDRs are distinguished (shown in red, dark red, orange and light brown) and are separated by reflectors R1, R2, and R3. The oceanic crust in shown light blue, and the syn-rift in dark blue.c) Line drawing of structure from the pre-stack depth migrated (PSDM) seismic line, this section has no vertical exaggeration.

Fig. 4. a) PSTM seismic reflection line with a vertical exaggeration of 5:1, the line location is shown in Fig. 1b**.** The black dashed line demonstrated the base of the isochore shown in Fig. 6b. b) Seismic line shown in a) with interpretation: the oceanic crust is shown in light blue, and the syn-rift in dark blue. In the area containing the SDRs and the LCVS four packages are distinguished and these are separated by reflectors R1, R2 and R3. c) Line drawing of structure from the pre-stack depth migrated (PSDM) seismic line, this section has no vertical exaggeration.

Fig. 5. Three seismic lines, a-c, showing the along-strike transition from the Laterally Confined Volcanic Succession to SDRs. The line locations are shown on the isochrons in Fig. 6. Reflectors R1 and R2 are annotated in each line, as are the stratal geometries in the package that they bound.

Fig. 6. a) vertical TWTT thickness map (an isochron) of the package shown in Fig. 5, which is bounded by reflectors R1 and R2 (Stage a). The three seismic lines (a-c) shown in Fig. 5 are also annotated and labelled here. b) isochron of the Stage c package which is defined as the SDRs overlying reflector R3. The base of this isochron is illustrated in both figures 3a and 4a.

Fig. 7. Three stage conceptual model for the 3D development of the LCVS and SDRs across the study area. a) shows basin evolution during stage a, as described in the text. b) shows basin evolution during stage b. c) shows basin evolution during stage c. For each stage the colours relate to those shown in earlier figures (Fig. 3, Fig. 4, Fig. 5). Each stage of margin evolution is represented by two representative cross-section reconstructions (i and ii), and one sketch map (iii). Cross section i) demonstrates the evolution of the seismic reflection line shown in Fig. 4 which is characterised by the occurrence of a rift-jump and the preservation of the LCVS.

Cross-section ii) shows the evolution of the seismic line shown in Fig. 3, which was characterised by continuous SDR emplacement through time.

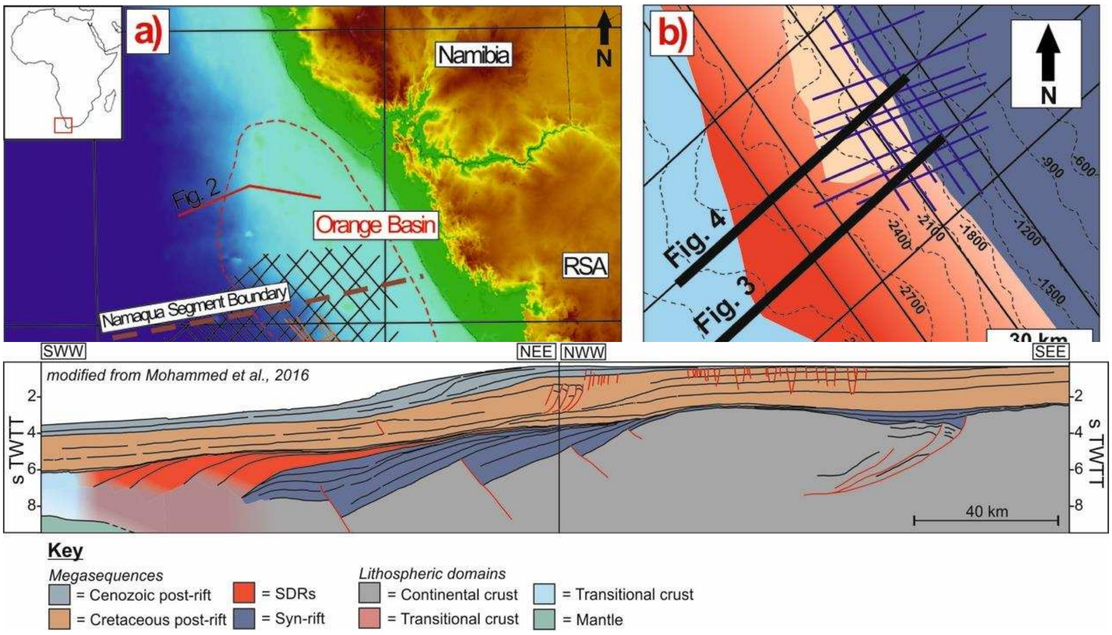

Figure 1 (colour)

Figure 2 (colour)

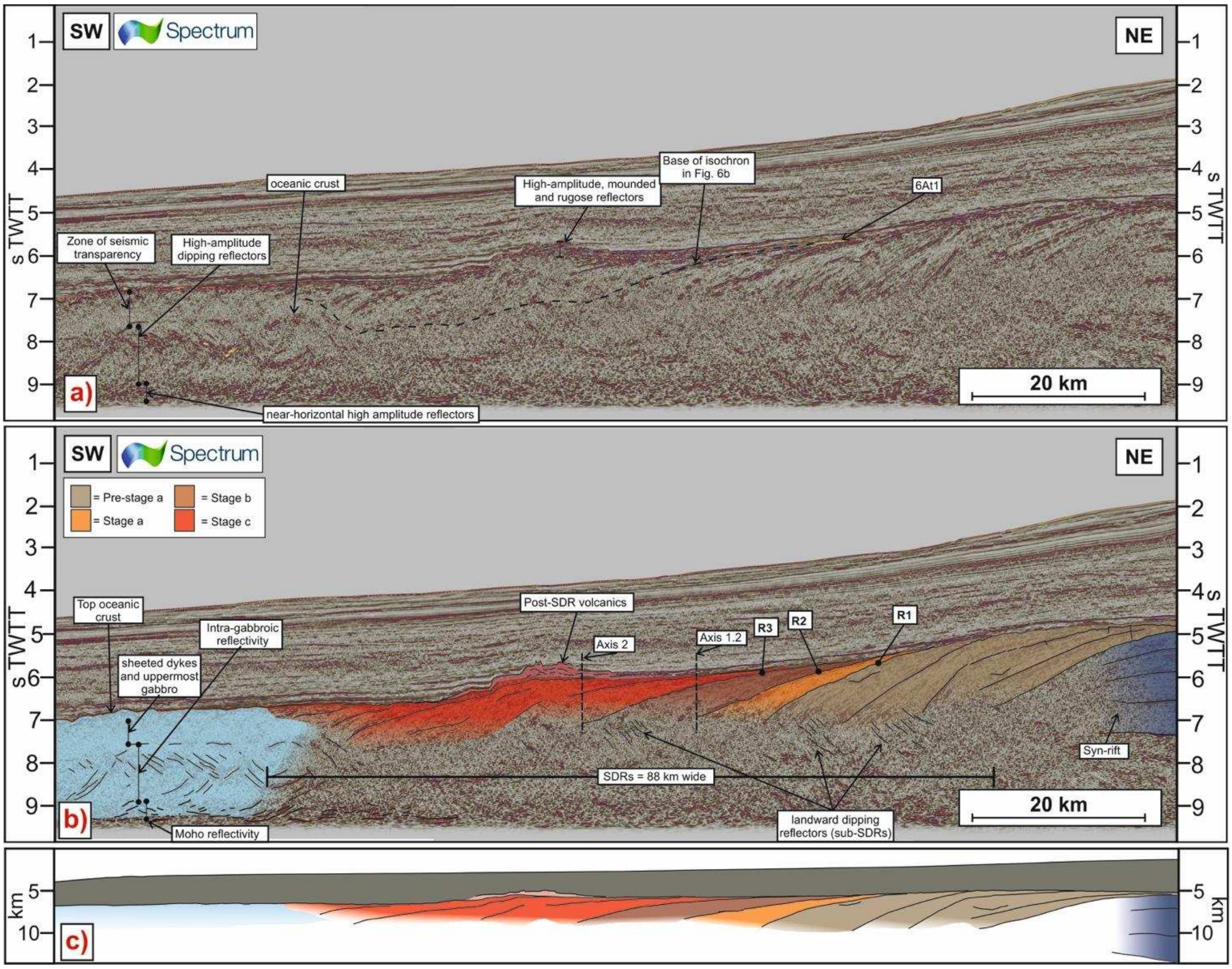

Figure 3 (colour)

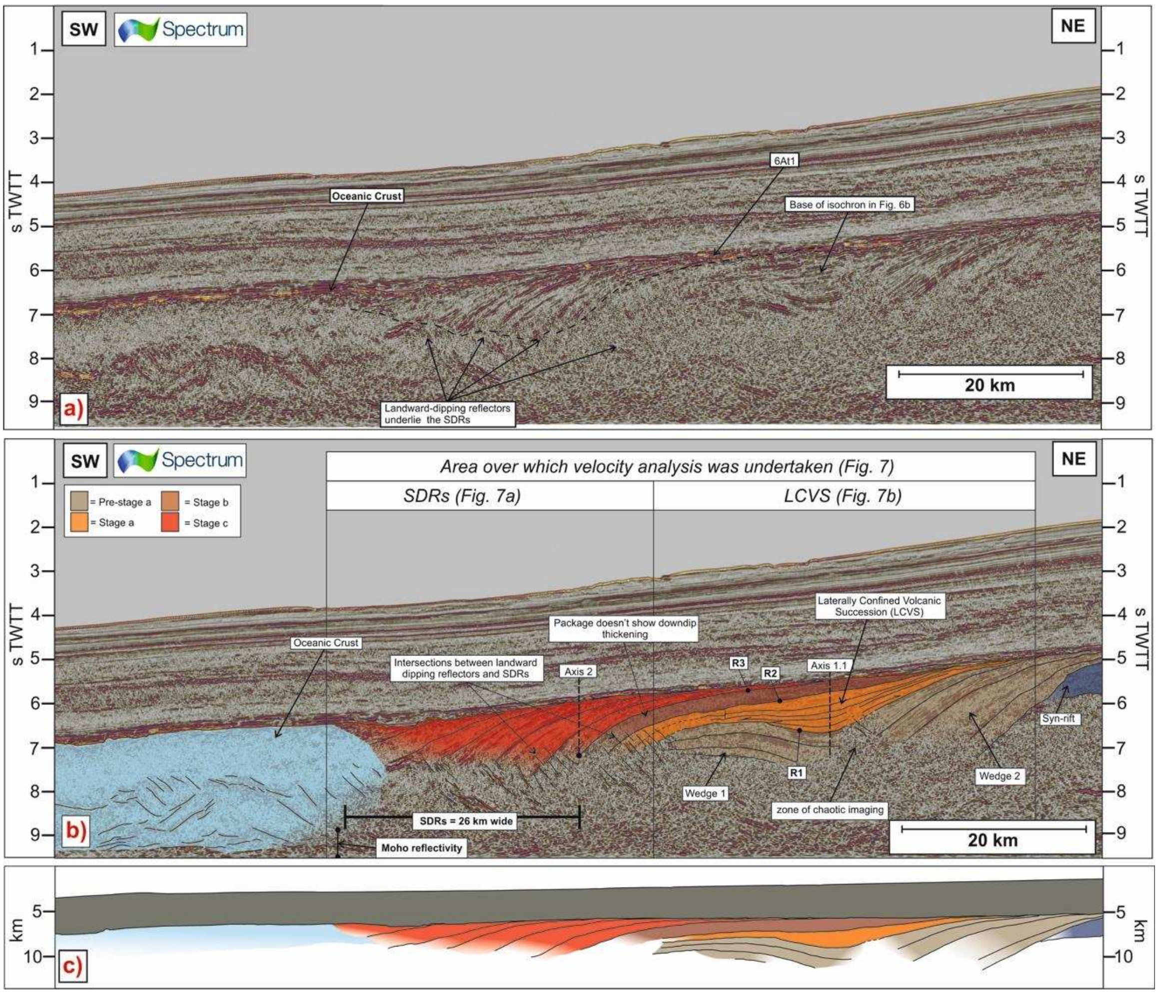

Figure 4 (colour)

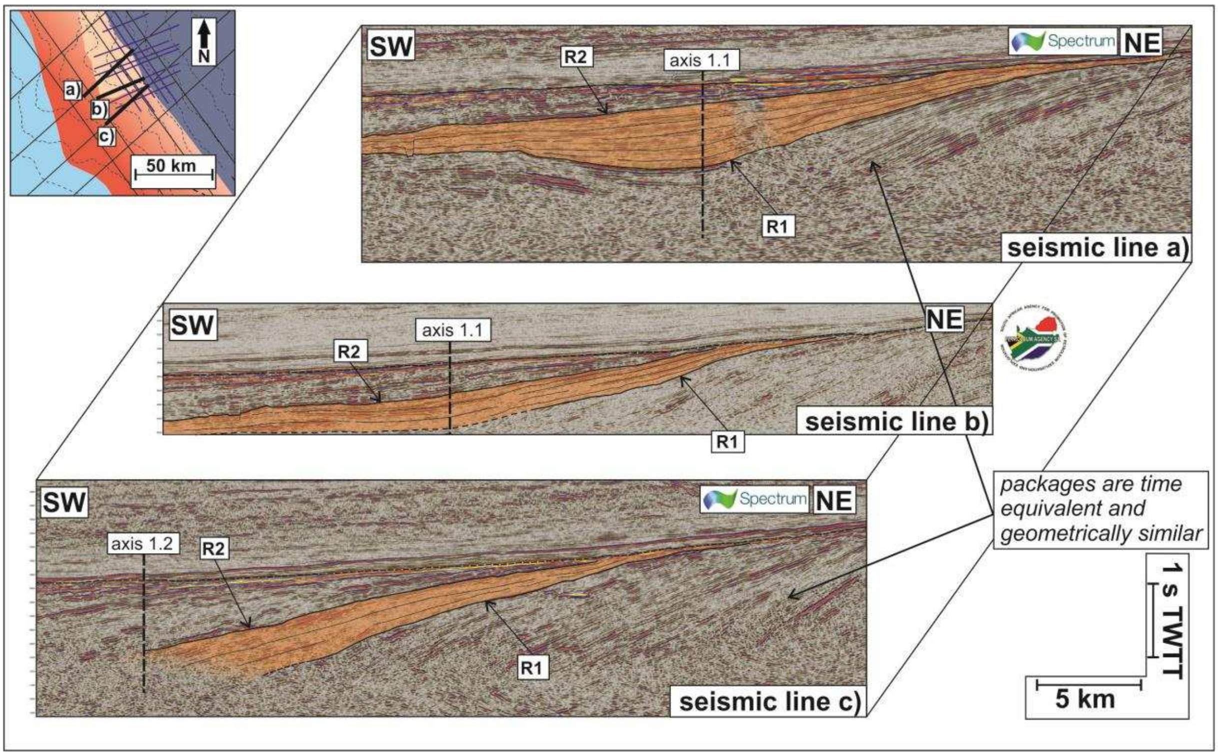

Figure 5 (colour)

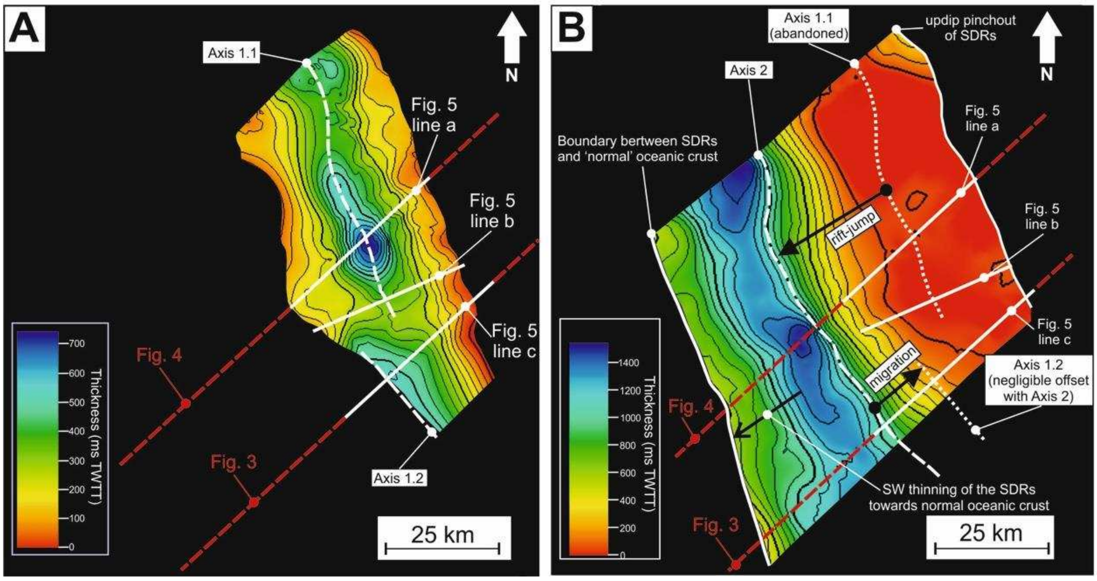

Figure 6 (colour)

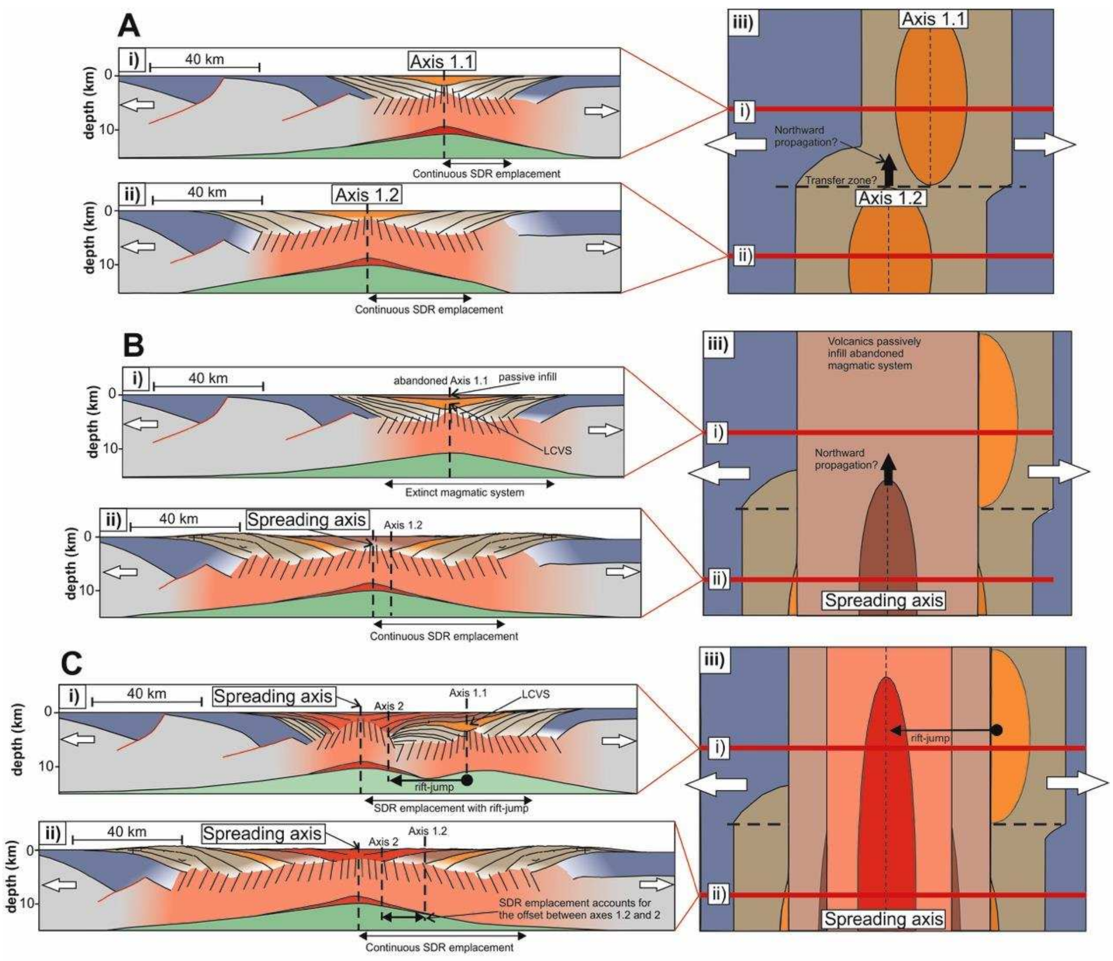

Figure 7 (colour)